Characterization of Influences on the Wall Stability of Deep Drawn Paperboard Shapes

Marek Hauptmann * and Jens-Peter Majschak

Deep drawn shapes with orthogonal wall components are usually evaluated by shape accuracy and visual quality. There have been only a few investigations on the stability of such structures; however, the effect of the wrinkles on the stability of the wall is important for packaging applications and can support the shape accuracy. This paper focuses on the influences of process parameters on the stability of orthogonal walls of shapes produced by deep drawing with rigid tools and immediate compression. The wall stability was evaluated by tensile testing orthogonal to the direction of the wrinkles. The stability distribution was characterized with regard to the drawing height, and a comparison was made between the two different materials. The wall stability decreased with increases in the forming height. Furthermore, a blank holder force design and z-directional compression level improved the wall stability. Together with an elevated moisture content of the material and thermal energy supply that delivered two to three times higher resistance against wrinkle extension, these effects drastically improved the wall stability.

Keywords: 3D-forming; Deep drawing; Paperboard; Stability

Contact information: Department of Processing Machines and Mobile Machines, Technische Universität Dresden, Bergstrasse 120, 01069 Dresden, Germany;
** Corresponding author: marek.hauptmann@tu-dresden.de*

INTRODUCTION

Packaging is one of the main applications of paper and paperboard materials. This field is continuously experiencing technological advances that are driven by the global consumer goods market. Packaging has expanded beyond its single functional role of enabling transport and providing the basic protection of goods. Beyond its basic functions, including the protection from mechanical, atmospheric, or biological load, the packaging is optimized to serve as multisensory sales and advertisement medium but also needs to have an ecologically optimized and economically feasible materials strategy. From the ecological point of view, paperboard has gained new interest as a packaging material because it is structurally light with high stiffness and durability. Paperboard has a high energy uptake potential in the event of compression, and print/advertisement can be applied to it. Moreover, decomposition options for paperboard are environmentally-friendly and include biodegrading and recycling, both of which are strongly desirable and widely accepted by the consumer. Several major drawbacks so far include its limited formability to complex shapes or the combinations of shapes, and advanced protection functions, *e.g.*, as a gas barrier.

The three-dimensional (3D) forming technology of paperboard is currently considered as a key enabler for a further increase in usage of paper and paperboard in packaging because recent scientific research has shown significant progress in 3D paperboard products giving confidence on their widespread application. A new level of

quality in deep drawn paperboard structures was reported by Hauptmann and Majschak (2011); the corresponding shapes showed sharp cylindrical geometries with a significant reduction in the visual defects and only minor deviations in shape. The deep drawing process used rigid tools and immediate compression after the material has entered the cavity. Investigations by Östlund *et al*. (2011) provided the first insight into the related 3D-forming process of hydroforming, which was further explored by Linvill and Östlund (2015). Linvill and Östlund (2015) used a moisture- and temperature-dependent constitutive model to show that friction was the main issue during hydroforming. From a materials standpoint, Vishtal *et al*. (2013) claimed that the requirements needed for peak performance in both processes were very different. Fiber modifications, introduced by Zeng *et al*. (2013), or chemical modifications, for instance through the use of gelatin (Khakalo *et al*. 2014) or PLA-latex (Svensson *et al*. 2013), lead to a high extensibility, which is most desirable for hydroforming. Meanwhile, Hauptmann *et al*. (2015) showed that an increased pore volume and reduced bonding capacity of the material will lead to improved formability in deep drawing with rigid tools. A third type of 3D-forming process has been investigated more thoroughly in recent years. The press molding process of paperboard provides tray-like shapes suitable for frozen or microwavable food preparation. The basic influencing parameters affecting the 3D-folding of paperboard tray-like shapes have been elucidated by Leminen *et al*. (2013). Others have described the effect of mold clearance (Tanninen *et al*. 2014) and new heating solutions for paperboard tray-like products (Tanninen *et al*. 2015), thus providing detailed information about the design of the creasing line pattern usually applied to the blank before press molding. The 3D-forming process of paperboard-polymer laminates was also made possible. Hauptmann *et al*. (2013) showed that deep drawn structures can be sealed tightly without creating pinholes that are likely to occur in wrinkled areas at the sealing rim. These pinholes are also known to prevent gas leaks in press molded trays; however, Leminen *et al*. (2015) found that the optimized blank holder force can lead to gas-tight sealed trays made from press molding.

Thus far, the highest forming ratio was achieved by deep drawing with rigid tools and immediate compression, although wrinkles cannot be avoided. It seems clear that wrinkles represent breaks in the material. Therefore, even if the material has not been ruptured, the wrinkled wall appears less stiff than the basic material. Consequently, one of the most desirable properties of the material is notably affected by the forming process.

A first basic screening on influencing parameters was introduced in Hauptmann and Majschak (2011). The overall tensile work, when the wrinkles were stretched until breakage, was investigated under different parameters using the deep drawing method. Moisture and weight were the main influencing factors. However, the tensile work was not suitable to compare the impact parameters because material with higher weight also exhibited higher basic tensile strength. Furthermore, the range of parameter values for thermal energy supply and blank holder force introduced in Hauptmann and Majschak (2011) could be increased. Constant blank holder forces were found to be the initial improving factor on the quality of deep drawn paperboard structures. However, it is believed that the blank holder force has only a minor influence on the fixation of the wrinkles, which is important for the stability of the wall of 3D structures. Recent investigations have shown further drastic improvement in visual quality of 3D structures using blank holder force trajectories adapted to the endurable load of the material (Hauptmann *et al*. 2015a). The concept of an increased blank holder force might have an effect on the deformation mechanisms in the material, which also affects the wall stability. The impact of this concept on the fixation of wrinkles in the wall should be investigated in

detail with regard to the two deformation phases introduced in Hauptmann *et al*. (2015b). The objective of this paper was to characterize wall stability and the influencing parameters that could improve wall stability with respect to the new blank holder force designs and in a broader range of thermodynamic parameters.

EXPERIMENTAL

Materials

A commercial 3-ply virgin fibre material (Trayforma Natura) from Stora Enso (Imatra, Finland) was used at 350 g/m² for the variation of basic process parameters. A second material, BiCo (Hauptmann *et al*. 2015b), was used at 350 and 500 g/m². These amounts were chosen because the material contains virgin fibres and 20% bi-component (PET staple fibre with low melting PET sheath). These components improve formability in terms of better fiber-to-fiber mobility during deformation and higher pore volume.

3D-Forming Equipment

Deep drawing experiments were conducted using a deep drawing machine designed for laboratory investigations at Technical University Dresden (Fig. 1) with the physical conditions presented in Table 1.

Table 1. Basic Conditions of the Deep Drawing Machine

Max. punch force (kN)	Max. blank holder force (kN)	Max. speed of punch (m/s)	Blank holder force accuracy (N)	Elastic deformation of tools under full load (mm)
56	28	0.8	+/- 70	< 0.02

The machine works with rigid tools and immediate compression inside the tools. The punch is controlled by positional regulation, while the blank holder converts from position to force regulation as soon as it makes contact with the paperboard. The blank holder force varies with the trajectory in relation to the punch position.

Fig. 1. Deep drawing machine and tool structure

The cavity and blank holder are polished, but the punch has a rougher surface to ensure the guidance of the material inside the tool. The cavity is coated with titanium nitride and polished after coating. All experiments were conducted with the same cylindrical geometry with a diameter of 110 mm and an orthogonal wall radius of 0.2 mm.

Influencing Parameters Included in the Experiments

The experiments included five parameters (thermal energy, moisture, drawing clearance, cone angle and blank holder force) that were maintained at various levels during the deep drawing process (Table 2). The thermal energy was varied by changing the tool temperatures, while keeping the temperature difference between both tools constant at 40 K. The time of energy intake from the tools was maintained at a constant speed of 20 mm/s during forming.

Table 2. Deep Drawing Parameters and Variation Range

Cavity/Punch Temperature (°C)	Paper-board Moisture (%)	Drawing Clear-ance (mm)	Cone Angle (°)	Blank Holder Force	Material (g/m²)	Drawing height (mm)
120/80	8	0.45	0.5	Constant	TF 350	25
200/160	12	0.4	0.3	Rupture optimized	BiCo 350	50
		0.3	0		BiCo 500	

Because the moisture of paperboard has a significant influence on wall stability in terms of increased resistance to wrinkle stretching, this parameter was included in the experiments. The moisture content was determined by weighing the samples in a normalized climate (23 °C, 50% humidity) delivering 7.9 ± 0.4% moisture. The samples were stored in a climate chamber at 30 °C and a relative humidity of 85%, while providing 12 +/- 0.6% moisture compared with their oven dry weight (EN ISO 287 2009).

The adjustment of the compression levels was reached by the use of different punches. Therefore, the drawing clearance and the cone angle of the punch were adjusted. The known recommendations for the compression expressed by the ratio of drawing clearance related to material thickness ranged from 0.5 and 1. However, not all of the materials showed a thickness reduction to a value of half their basic thickness, and some of the 3D-structures exhibited discoloration. The drawing clearance and the cone angle of the punch were adjusted simultaneously. The arrangement of the clearance and cone angle demonstrated the geometry of the three different punches used to increase the compression and its distribution over the drawing height (Table 1). The investigations with the Trayforma Natura (TF) material should provide insights into the impact of basic parameters. For this material, the maximum compressive ratio of 0.67 (drawing clearance of 0.3 mm with material thickness of 0.45 mm, referred to as compression level 1) was determined to be feasible before defects (ruptures) occur as a result of high compression.

The blank holder force was investigated using two different designs; a constant blank holder force was used as a reference and was compared with a rupture optimized design (Hauptmann *et al*. 2015a). The design was adjusted according to elevations in temperature, compression, or moisture. Figure 2 displays the applied designs that made use of the full blank holder force capacity with each parameter combination. The accuracy of

the force control was sufficient, and the force curves are accurately realized, as shown in the example of the two measured curves of TF material at a clearance of 0.45 mm with constant and rupture optimized design (Fig. 2).

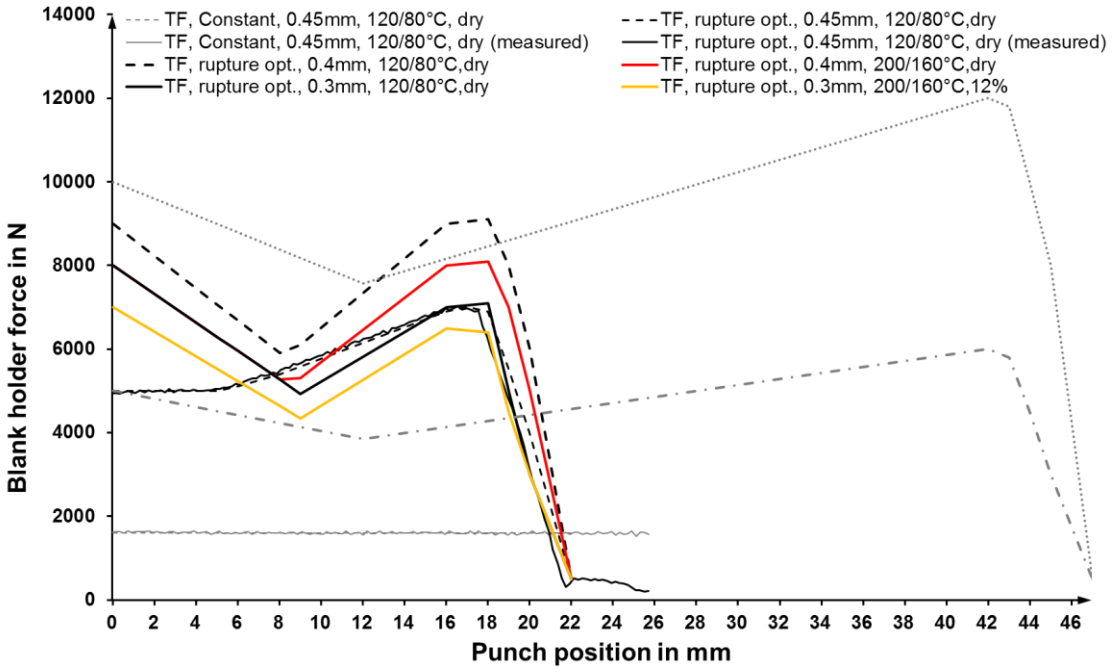

Fig. 2. Blank holder force design, as specified by Hauptmann *et al*. 2015a with modifications according to forming conditions listed in Table 2

Evaluation of Wall Stability

The wall stability was evaluated by determining the tensile behavior of the material orthogonal to the wrinkles. Therefore, the specimens were cut from the wall of 3D-structures and loaded until breakage (Fig. 3).

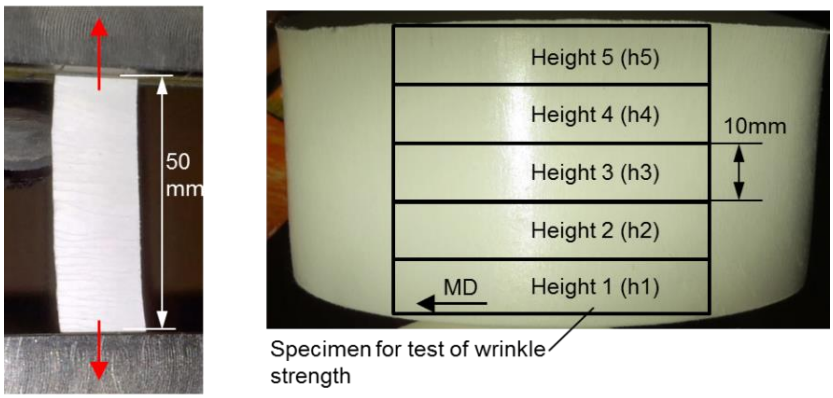

Fig. 3. Arrangement of specimens cut from the wall of 3D-structures. The example is a 50-mm wall.

The specimens were sectioned from the wall, which was stretched in the cross direction of fiber orientation (CD). The wrinkles, in this case, have to form out against the machine direction (MD), leading to an increase in the distance between the wrinkles and a

less uniform distribution of wrinkles. That means the material network was loaded in MD during tensile testing after the wrinkles were stretched out. The width of the specimens was set to 10 mm because a greater width leads to an increase in non-uniform load distribution during testing. A continuous increase in the excess material leads to a difference in the extensibility from one border to the next, which can be followed through a consideration of the characteristic triangles describing the material excess. The specimens were cut from the wall at different heights to cover the two phases of deformation, as specified in Hauptmann *et al*. (2015b), and to demonstrate the impact of the parameters on both phases. The tensile tests were conducted on a standard tensile test machine (Zwick Roell Z020, Ulm, Germany) with a free length of 50 mm and a speed of 20 mm/min. The free length was reduced from the standardized tensile testing conditions because the longer stripes would lead to a mixture of MD and CD material behavior. The force sensor used in the experiments exhibited a maximum force generation of 5 kN, and the calibration delivered an inaccuracy rate of 0.2 to 0.35% in the range of 20 to 250 N.

RESULTS AND DISCUSSION

Influence of the Drawing Height

As a reference point in the tensile tests of wall stripes, TF material was tested with constant tool temperatures, a low compression and moisture level, and a constant blank holder force at height level h1 (nearest to the border) of a 3D-structure of 25 mm drawing height. This test delivers the force curve shown in Fig. 4a. After five repetitions, an acceptable standard deviation was achieved, which confirmed the reproducibility of the results.

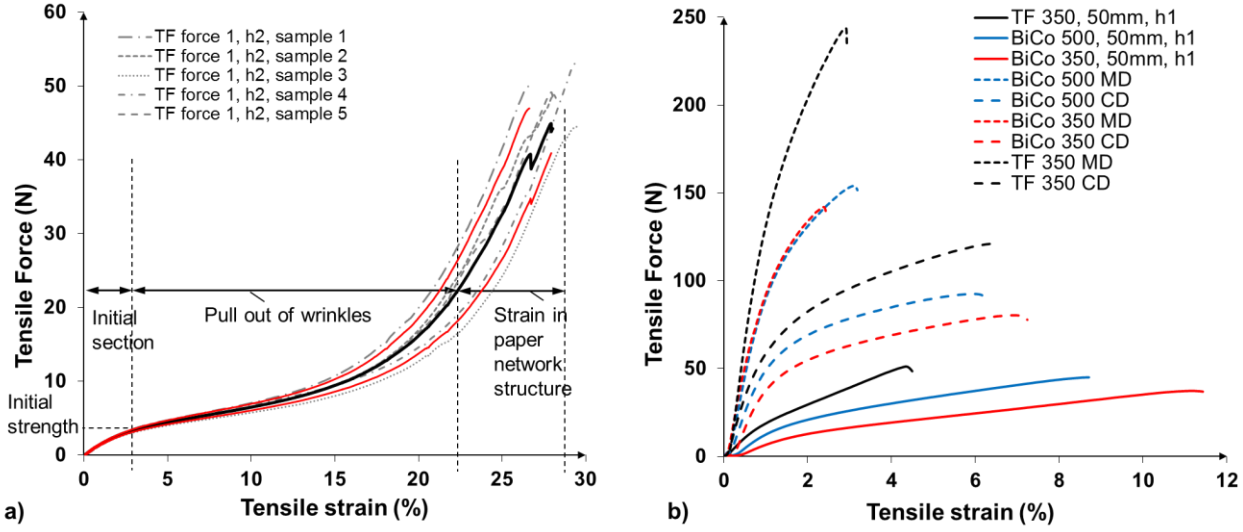

Fig. 4. a) Tensile force curves of specimens cut from the wall of a 25 mm high 3D-structure from height level h2, deep drawn at 120/80 °C, 0.45 mm clearance, 1600 N constant blank holder force, and 8% relative moisture. Standard deviation is indicated by the red curves. b) Comparison of tensile characteristics of formed wall structures (dashed lines) and unformed material (solid lines) with the following forming conditions: 50 mm wall height, 0.4 mm clearance, 120/80 °C, 8 % moisture and rupture optimized blank holder force

The curves do not show the typical tensile behavior commonly seen in the basic paperboard, even not at lowest height level, because of the wrinkles, which were pulled out during the test (Fig. 4b). After an initial force, the force level followed a very flat incline, which characterized the separation of the wrinkles. Within the curves at elevated height levels, the force increased progressively near the end of the tensile test when the material reached a breaking point (Fig. 4a). In this last section, the basic material network structure was strained to its maximum limit. The tensile strength reached before breakage was significantly lower than the tensile strength of the base board (Fig. 4b), even at the lowest height level near the bottom, where only few wrinkles occurred. This effect could have two different reasons. The material is strained along the forming height near to its maximum including high plastic deformation already exceeding the strain values determined in a uniaxial tensile test. Biaxial strain should not decrease the maximum achievable strain in one of the directions (Gundersen and Rowlands 1983), but the concurrent z-directional compression apparently leads to higher strain rates and increased plastic deformation, which could cause damages in fiber bonding. Another reason could be the seen in the wrinkles. The failure mechanism at wrinkles is not accurately understood so far. The failure could be described as an instable compression breakage comparable to buckling. The investigations introduced by Hauptmann *et al.* (2015) indicate that the bending properties of the material show a systematic correlation to the formability in deep drawing with immediate compression. The nature of a bending break is mainly characterized by the compressive failure on the concave side of the curvature and the damage is more present at the compression side until reaching the neutral span; the tension side stays intact (Carlsson *et al.* 1980). In both of the cases wrinkles represent weak points in which the bonds were reduced significantly and the structure has already experienced damages. This reduces the tensile strength and the bending stiffness of the wall.

The strain at break was nearly 28% at the forming height of 15 to 25 mm, which is significantly higher than those of base board (3% in MD) because of the extensibility of the wrinkled areas. A test of a 3D-structure with 50 mm drawing height allowed an analysis of the extension behavior on five levels of drawing height. The results showed that the initial force needed to begin stretching out the wrinkles decreased rapidly with increasing forming height (Fig. 5a). This effect can be described by the initial slope of the curve, which also decreased considerably with increasing forming height. Furthermore, the force during the stretching out of the wrinkles increased, such that it could be described by the slope of the curve after having passed the initial section (Fig. 4). There is also a difference between the recorded curves at the same height level, cut out of a 25 mm (gray curves) and a 50 mm 3D-structure (black curves). The differences in the maximum strain could be attributed to the origin and positioning of the specimens because the specimens from the 25 mm and 50 mm walls were cut starting from the border. Thus, h1 was reached at 5 mm from the bottom for the 25 mm wall and directly at the bottom for the 50 mm wall. In reality, this displacement was smaller, as the 50 mm high wall was stretched during the process to 56 mm, while the 25 mm wall was stretched to 27 mm, leading to a displacement of only 1 mm. However, in a range of 3 to 15 mm, the higher force of the curve for specimen from 25 mm wall at height level h2 cannot be explained by this reason alone. A higher blank holder force, which was applied to the 25 mm high samples, increased the resistance against wrinkle stretching.

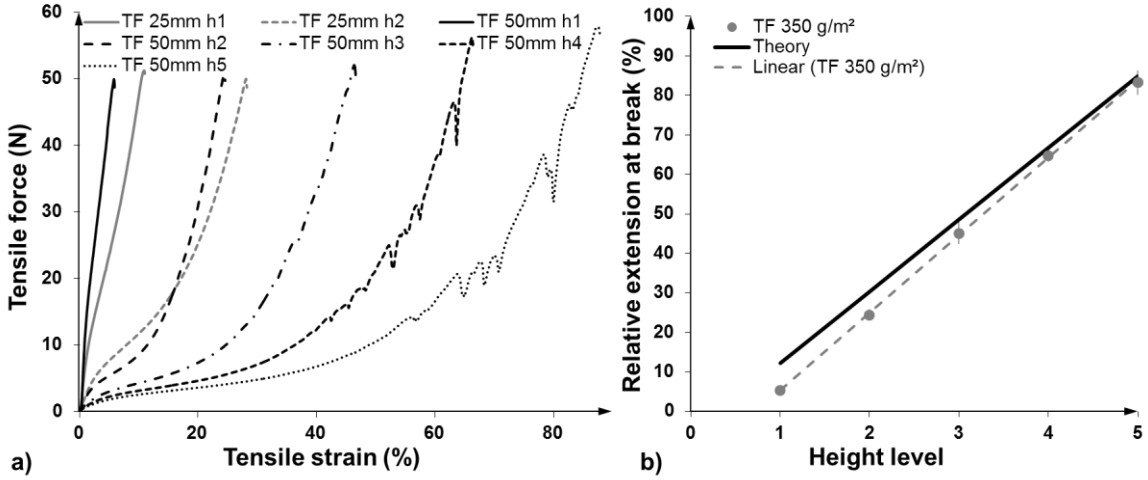

Fig. 5. a) Tensile force curves of different height levels cut from 25 mm and 50 mm high samples from TF material with 350 g/m², deep drawn with tool temperatures of 120/80 °C, 0.4 mm clearance, 8% moisture, and a rupture optimized blank holder force; b) relative extension at break referring to the 50 mm high sample from a) on height levels h1-5 for 50 mm sample compared to theoretical circumference increase

The strain at break systematically increased with each height level. The increase followed a linear trend (Fig. 5b). The theoretical extension potential is described by an increase in the material excess and depends on the drawing height. The material excess was proportional to the increase of the blank circumference drawn into the cavity and reduced to the circumference of the base geometry. A theoretical relative extensibility (ε_{theor}) was calculated with a cavity radius (D_c), a deep drawn height (h), and strain at break of the base board (ε_b), as follows:

$$\varepsilon_{theor} = \frac{(D_c+2\cdot h)-(D_c\cdot\pi)}{(D_c\cdot\pi)} \cdot 100 + \varepsilon_b \quad (1)$$

The measured relative extension of TF (350g/m²) drawn to a height of 50 mm was similar to the theoretical value, especially near the border (h5). It was assumed that the difference between the calculated and measured extension was generated by a compensation of the material excess through fiber-to-fiber movement, but it is not clear which role compression played. It is likely that the extension of the compressed material was different than the extension of uncompressed material.

Furthermore, a decline in the local force was recognized at a relative extension above 50%. The origin of this effect could be delaminating damage in between the 3 material layers at the site of the wrinkles, starting with this level of excess material.

Influence of Material

The BiCo material showed that the basic tendency of extension with increasing forming height was transferable between different materials (Fig. 6a). The increase was also nearly linear, but the regression function had a significantly lower incline (Fig. 6b), indicating an increased capacity of the material to compensate for the material excess. The distance between the calculated and measured extension increased continuously, resulting in compensation for increasing height level for the excess material.

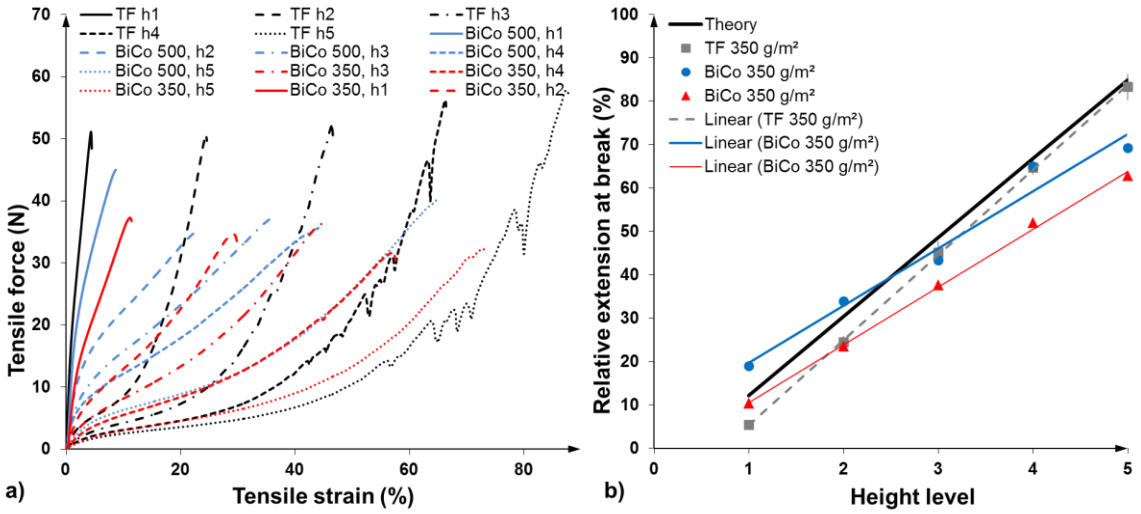

Fig. 6. a) Tensile force curves of different height levels cut from 50 mm high samples deep drawn with tool temperatures of 120/80 °C, 0.4 mm clearance, 8% moisture, and a rupture optimized blank holder force, using TF 350 g/m² or BiCo in 350 g/m² or 500 g/m² material in comparison; b) relative extension at break for TF 350 g/m and BiCo in 350 g/m² and 500 g/m² at height levels h1-5 for 50 mm samples with the same conditions as in a)

The higher extension values within lower height levels could be explained by a higher strain of the wall, which nominally should be 50 mm. The measured wall height of the 3D-structure of TF 350 g/m² was 56 mm in CD. The wall height of the BiCo material was similar with both grammages but higher than measured with TF material (60 mm). This means that the specimens shifted in their positioning relative to the bottom at lower height levels for around 4 mm, which already might have yielded different results. The break in the BiCo material was not a typical sharp break at one position; it exhibited the characteristics of a delaminating break with a long break area (Fig. 7a).

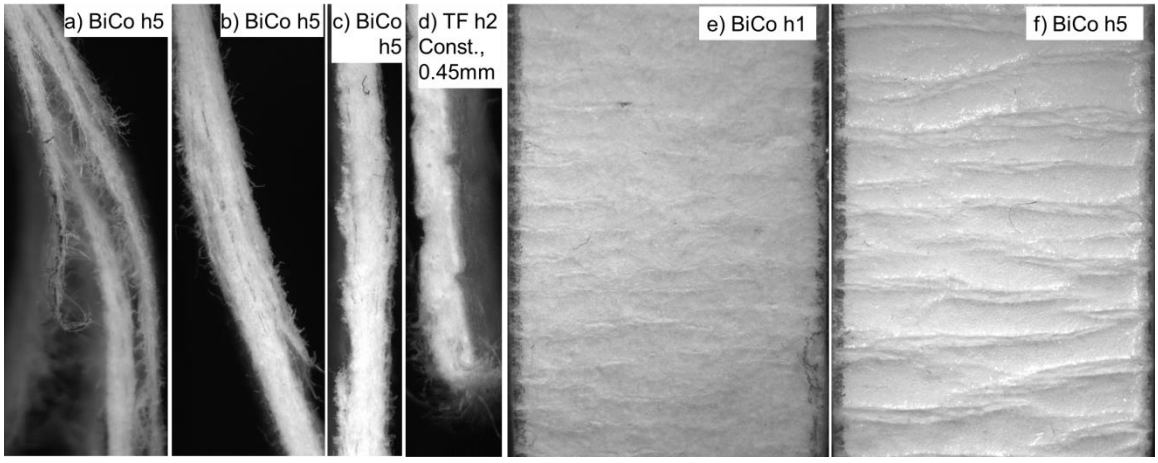

Fig. 7. Images of breaks and surface quality of specimens after the tensile test

The elongation, in this case, might not have been only generated by the stretching of wrinkles and strain in the network, but also from continuous partial breakage. Other sections of the same specimen showed delamination, even if the section was not broken (Fig. 7b). To some extent, this was expected because the material was designed to allow

for fiber-to-fiber displacement. When considering the failures at wrinkles as a bending failure as described by Carlsson *et al.* (1980), the alternating breakage caused by compression on both sides of the material (wrinkles appear on both sides) would lead to a higher risk for failure in both, top and bottom layer and the material in the middle layer experiences least damages. This would support the delamination failure shown in (Fig.7a) especially if the material is made of nearly uniform pulp composition. In case of the usage of layer structures using different pulp compositions the breakage could look different as can be seen from Fig. 7 c) and d).

The wrinkles were different in the BiCo and TF materials. The TF material exhibited a clear rectangular pattern in the cross section (Fig. 7d), but the wrinkles were not clearly identified in the BiCo samples (Fig. 7c). Ruptures in the TF material appeared at the site of the wrinkles, and the rupturing caused a connecting line through the thickness between the wrinkles on both sides (Fig. 7d). The surface of the specimens showed elongation of the wrinkles, and they increased with the drawing height (Fig. 7e and f). Considering that there were almost no visible wrinkles in the samples made of the BiCo material, the images indicated that the material structure was damaged at the site of the wrinkles when they were pulled out of the structure.

The initial force values of the BiCo material of 350 g/m² were significantly higher than those of the TF material of the same weight at height level 2 (h2). Initially, the force curves demonstrated that the force was drastically higher for the BiCo material. Only the first height level exhibited a lower force, which was expected because of the lower basic tensile strength of BiCo compared to TF (141 N in MD for BiCo 350 g/m², 153 N for BiCo 500 g/m² and 249 N for TF). With elevated height, the force level achieved in the tensile test increased drastically. This increase in the first part of the force curve is considered advantageous for wall stability because it describes the resistance against deformation from the target shape. The reason of this increase is likely to be achieved by the fiber network deformation during the in-plane compressive loading phase. The maximum force at break was considerably lower for BiCo compared to TF, which was also expected because of a lower basic tensile strength of the material.

Influence of Blank Holder Force

The variation in the blank holder force from a constant value of 1600 N, which is the maximum endurable constant force with the lowest compression level, is shown *via* a rupture optimized force design (Fig. 2). The results showed an improvement in wall stability (Fig. 8).

The higher force level exhibited an increased initial slope, and the slope increased during wrinkle stretching, which can be considered as a remarkable effect compared to the extent of the standard deviation (indicated by the grey dotted curves) in these two most important sections. The effect of the blank holder force occurred at both height levels, and it was comparable to an increase in the compression level achieved by a reduction of the drawing clearance from 0.45 mm to 0.4 mm, with concurrent reduce of the cone angle from 0.5° to 0.3°. These results support the findings from a previous study (Hauptmann *et al*. 2015b). Consequently, the increased blank holder force was also able to support the deformation in the fiber network taking place during the deep drawing process. However, these results must be evaluated in contrast with the other parameters influencing the wall strength.

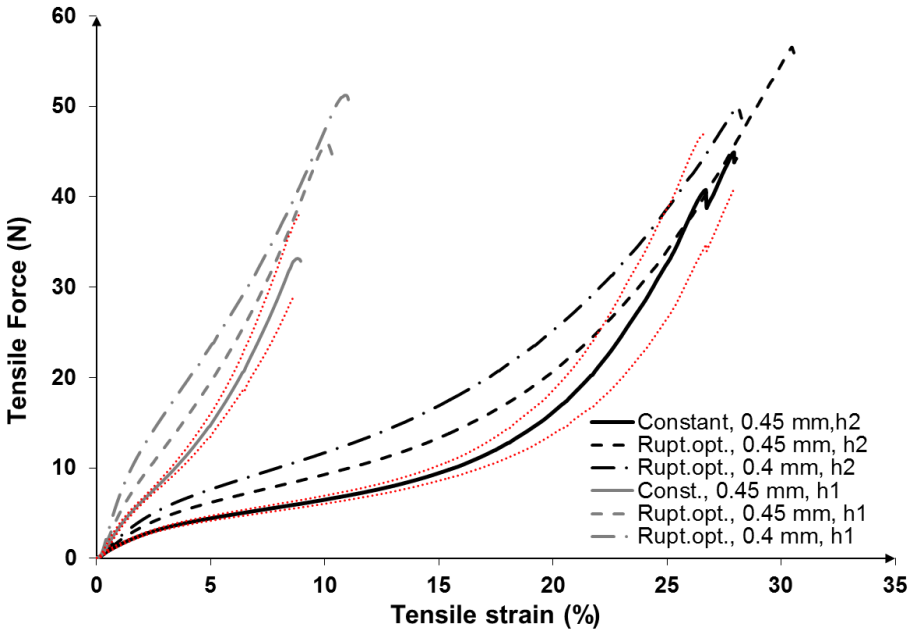

Fig. 8. Tensile force curves with varying compression (indicated by drawing clearance, see Table 2), blank holder force illustrate on two different height levels (gray height level 1 and black height level 2). Specimens were taken from a 25 mm high wall of samples from TF material deep drawn at temperatures of 120/80 °C using a moisture content of 8% of the material. Red dotted lines indicate the standard deviation on the example of the two solid curves.

Influence of Thermodynamic Parameters

The known parameters that influenced the thermodynamic situation in the material are moisture content, thermal energy intake, and compression. It is likely that these parameters influenced the wall strength and interacted with the blank holder force level. The variation of these parameters provided insight into their impact on the tensile force characteristics (Table 2; Fig. 9).

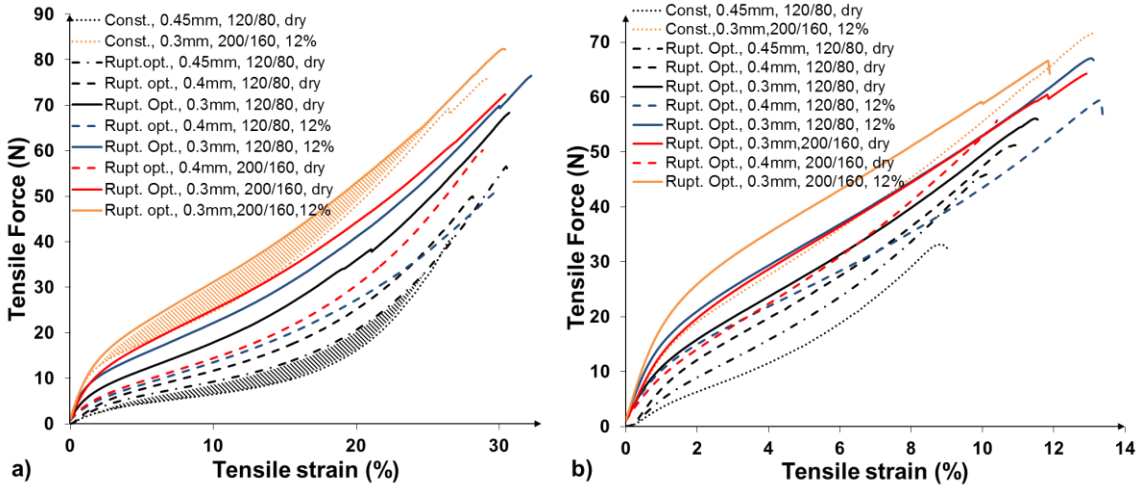

Fig. 9. Tensile force curves of 25 mm high samples from TF material, with a variation in the thermal energy, compression, blank holder force design, and material moisture (see also Table 3) on a) height level h2 and b) height level h1

Table 3. Explanation of the Use of Color and Line Types in Relation to Parameter Variation in Fig. 9

Blank holder force		Compression level	
Dotted line	Constant force	Low (0.45mm clearance)	
Other line	Rupture optimized force design	Medium (0.4mm clearance)	
		High (0.3mm clearance)	
Tool temperatures		**Moisture**	
Red color	High temperatures at 200/160°C	Blue color	High moisture at 12%
Other color (except orange)	Lower temperatures at 120/80 °C	Other color (except orange)	Lower moisture at 8%
Orange color high moisture and high temperature levels			

Elevated moisture (blue curves) and tool temperatures (red curves) did not show a notable effect in the tensile strength characteristic of the wall, without a concurrent increase in the compression level. An increase in the compression level, without an elevated moisture and temperature, already demonstrated a major effect, as shown by the 0.45 mm clearance with dotted line, 0.4 mm dashed line, and 0.3 mm solid line, especially with regard to the black curves (indicating the lower level for moisture and thermal energy intake). This effect was more intensively recognized at height h2 (Fig. 9a) compared with height h1 (Fig. 9b), which was expected because the concurrent reduction of the cone angle increased the compression progressively with increasing wall height. The compression led to a reduction in the distance between the fibers, and consequently, a higher number of potential sites for new bonding. Furthermore, the heat transfer to the material was supported by a higher compression, which might induce an increased z-directional plastic deformation. Elevated heat and moisture alone do not induce new hydrogen bonds, if there are no new contact sites between fibers. Hydrogen bonds are believed to be one of the major bonding mechanisms (Hubbe 2007), and they require a distance of not more than 0.27 nm (Linhard 2005). In combination with compression, the situation is different. In this case, both elevated moisture and elevated heat independently provide a further increase in the resistance of the material against wrinkle stretching. The single effects are within the same range. A full combination of high parameter levels (orange force curve) delivered the highest possible force value and best wall stability. These results supported the idea that elevated moisture dried out by increased thermal heat supply leads to new hydrogen bond formation in an intensively compressed network structure, which provides new contacts between the fibers. The force level achieved with these experimental conditions was more than twice as high compared to the reference (dotted line curves). The major role of the compression furthermore suggests that mechanical interlocking, found to be another major bonding mechanism (Hirn and Schennach 2015), also is increased in the higher compressed material sections, especially at wrinkles. It must be emphasized that the initial resistance against wrinkle stretching increased by a factor of more than three. This effect was most desirable because deformations larger than 1.0% represent a considerable deviation of the final shape. The influence of the blank holder force, in addition to the thermodynamically

induced effects, is still recognizable and also increases in combination with high levels of moisture, temperature, and compression. The orange shaded area describes the difference between constant and rupture optimized blank holder force design, with a higher level of thermodynamic parameters. This area is larger than the black shaded area describing the same step with lower levels of thermodynamic parameters. New bonds in the material were also created when using a constant blank holder force. This was indicated by the consequently higher maximum forces reached. The rupture optimized design achieved considerably higher force levels in the site where the wrinkles were stretched out. This confirmed that the elevated blank holder level, adapted to the endurable load of the material, helped to exploit the material deformation and its fixation potential. A comparative visual evaluation of the specimens of the reference (constant blank holder force, low levels with all parameters) with the best achieved results using high levels for all parameters, revealed that the surface was modified by the process parameters (Fig. 10b).

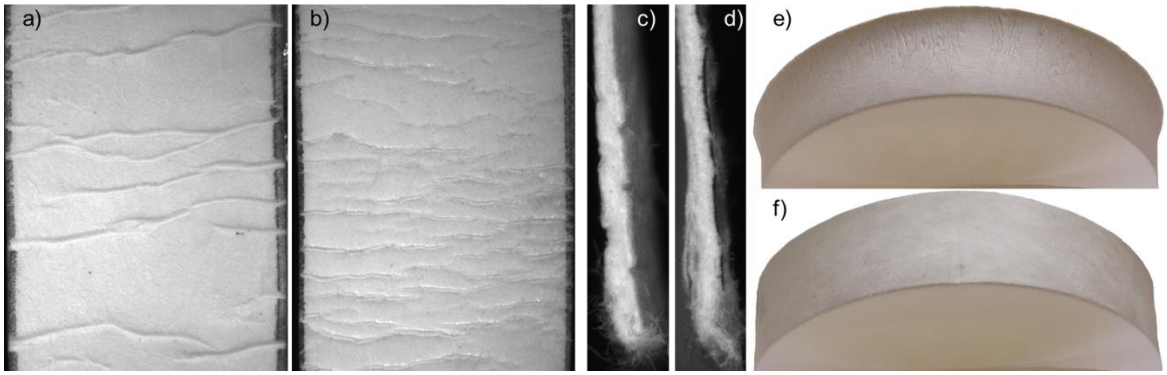

Fig. 10. Macroscopic images of specimens from height h2 and the corresponding 25 mm deep drawn shapes with a), c) and e) low levels for all parameters; b), d) and f) high levels for all parameters

A higher number of wrinkles were visualized in comparison to the reference (Fig. 10a). The cross section of the wrinkles did not show a rectangular pattern (Fig. 10d) like the reference (Fig.10c). Therefore, the extension provided by one wrinkle in the tensile test was reduced. However, the increasing number of wrinkles yielded comparable overall extension. The reduced local, in-plane displacements led to thinner wrinkles, which were finely distributed over the wall. This was likely responsible for the higher strength opposing the wrinkle stretching force. It can be assumed that increased plastic deformation was generated from thinner wrinkles.

Furthermore, the strain in the wall of 3D shapes along the drawing height increased considerably within the parameter variation. The reference samples exhibited a wall height of 26 mm (in CD), and the corresponding strain was 4.0%. The samples produced with high parameter levels overall, provided a wall height of 28 mm (CD) and a strain of 12%. The thickness of the wall following a slight linear incline over the forming height was reduced. The reference samples showed a linear thickness characteristic from 0.48 mm to 0.65 mm, while the samples with the highest parameter levels provided a thickness of 0.30 to 0.37, linearly increasing from the bottom to the border. The decrease in the thickness was dependent upon the compression level, as elevated moisture content and heat rate produce identical thickness profiles at the same compression level. Both effects suggested a reduction in the wall stability. The increased strain resulted in a slightly (2 mm) shifted

position; if the specimens were cut out, this effect would lead to lower force values in the tensile test. However, the opposite effect was measured, underlining the importance of the thermodynamic parameters with respect to wall stability. The decreased thickness also suggests a reduced bending stiffness of the wall; however, the wrinkles created damage to the walls, reducing the stiffness more intensively. The resistance against wrinkle stretching was unaffected by the reduced thickness.

CONCLUSIONS

1. The wall stability, expressed by the resistance against wrinkle stretching of the 3D structures by a tensile test orthogonal to the wrinkles, decreased systematically with the forming height, while the elongation increased linearly with the forming height.
2. An adapted blank holder force was used to maintain highest possible surface pressure on the material until it was drawn out of the blank holder. This method significantly improved the wall stability and supported the exploitation of the material fixation capacity, resulting in elevated moisture, tool temperature, and z-directional compression.
3. Material with improved deformation potential in terms of fiber-to-fiber movement and an increase in weight had increased wall stability.
4. The z-directional compression of the wall inside the tools had a major influence on the wall stability. Higher compression force improved wall stability.
5. Superimposing high compression (at a compression ratio of 0.67) with elevated moisture (of 11 %) and thermal energy (through supply of tool temperatures of (200°/160°) led to the highest wall stability level, while increased moisture or thermal energy alone did not provide a considerable improvement in wall stability.
6. The application of the highest moisture content, temperature, and compression level increased the axial strain and reduced the thickness of the wall notably. This resulted in an improved forming degree without a reduction of the wall stability.

ACKNOWLEDGEMENTS

The authors gratefully acknowledge support from the German Research Foundation and the Open Access Publication Funds of the TU Dresden.

REFERENCES CITED

EN ISO 287 (2009). "Paper and board – determination of moisture content of a lot – oven-drying method," European Committee for Standardization, Brüssels, Belgium.

Hauptmann, M., and Majschak, J.-P. (2011). "New quality level of packaging components from paperboard through technology improvement in 3D forming," *Packaging Technology and Science* 24(7), 419-432. DOI: 10.1002/pts.941

Hauptmann, M., Schult, A., Zelm, R., Gailat, T., Lenske, A., Majschak, J.-P., and Grobmann, H. (2013). "Gastight paperboard package - A new step in food packaging," *Professional Papermaking* 1, 48-51.

Hauptmann, M., Wallmeier, M., Erhard, K., Zelm, R., and Majschak, J.-P. (2015b). "The role of material composition, fiber properties and deformation mechanisms in the deep drawing of paperboard," *Cellulose* 22(5), 3377-3395. DOI: 10.1007/s10570-015-0732-x

Hauptmann, M., Weyhe, J., and Majschak, J.-P. (2015a). "Optimisation of deep drawn paperboard structures by adaptation of the blank holder force trajectory," *Journal of Materials Processing and Technolgy* (under review).

Khakalo, A., Filpponen, I., Johansson, L.-S., Vishtal, A., Lokanathan, A., Rochas, O., and Laine, J. (2014). "Using gelatin protein to facilitate paper thermoformability," *Reactive & Functional Polymers* 85, 175-184. DOI: 10.1016/j.reactfunctpolym.2014.09.024

Leminen, V., Tanninen, P., Lindell, H., and Varis, J. (2015). "Effect of blank holding force on the gas tightness of paperboard trays manufactured by the press forming process," *BioResources* 10(2), 2235-2243. DOI:10.15376/biores.10.2.2235-2243

Leminen, V., Tanninen, P., Mäkelä, P., and Varis, J. (2013). "Combined effect of paperboard thickness and mould clearance in the press forming process," *BioResources* 8(4), 5701-50714. DOI: 10.15376/biores.8.4.5701-5714

Linvill, E., and Östlund, S. (2015). "Parametric study of hydroforming of paper materials using the explicit finite element method with a moisture- and temperature-dependent constitutive model," *Packaging Technology and Science* (under review).

Östlund, M., Borodulina, S., and Östlund, S. (2011). "Influence of paperboard structure an processing conditions on forming of complex paperboard structures," *Packaging Technology and Science* 24(6), 331-341. DOI: 10.1002/pts.942

Svensson, A., Lindström, T., Ankerfors, M., and Östlund, S. (2013). "3D-shapeable thermoplastic paper materials," *Nordic Pulp and Paper Research Journal* 28(4), 602-610. DOI: 10.3183/NPPRJ-2013-28-04-p602-610

Tanninen, P., Kasurinen, M., Eskelinen, H., Varis, J., Lindell, H., Leminen, V., Matthews, S., and Kainusalmi, M. (2014). "The effect of tool heating arrangement on fibre material forming," *Journal of Materials Processing Technology* 214(8), 1576-1582. DOI: 10.1016/j.jmatprotec.2014.03.001

Tanninen, P., Leminen, V., Eskelinen, H., Lindell, H., and Varis, J. (2015). "Controlling the folding of the blank in paperboard tray press forming," *BioResources* 10(3), 5191-5202. DOI: 10.15376/biores.10.3.5191-5202

Vishtal, A., Hauptmann, M., Zelm, R., and Majschak, J.-P. (2013). "3D forming of paperboard: The influence of paperboard properties on formability," *Packaging Technology and Science* 27(9), 677-691. DOI: 10.1002/pts.2056

Zeng, X., Vishtal, A., Retulainen, E., Sivonen, E., and Fu, S. (2013). "The elongation potential of paper - How should fibres be deformed to make paper extensible," *BioResources* 8(1), 472-486. DOI: 10.15376/biores.8.1.472-486

Article submitted: December 9, 2015; Peer review completed: January 14, 2016; Revised version received and accepted: January 22, 2016; Published: February 1, 2016.
DOI: 10.15376/biores.11.1.2640-2654